A novel reservoir computing platform constructed by laser controlled GaAs resonator

Leisheng Jin*, *Member, IEEE*, Zhuo Liu and Lijie Li, *Senior Member, IEEE*

***Abstract*—In this work, a novel realization of the well known machine learning approach—reservoir computing (RC) using nanoelectromechanical system (NEMS) GaAs resonator is proposed. The specially designed resonator can interact with laser directly without cavity. Thanks to the richness of nonlinearity embedded in the light-mediated dynamical interacting process, the RC platform performs outstandingly even by eliminating the time delay feedback, and the conduction of nonlinear autoregressive moving-average (NARMA) task shows that the normalized mean square error (NMSE) can achieve 2.1×10^{-3} that is one order of magnitude lower than the recently reported result. Detailed theoretical modeling as well as numerical simulations on device's nonlinear dynamics and RC's hyperparameters are given. The interplay between the transient dynamics of the resonator and RC performance is particularly investigated.**

***Index Terms*—reservoir computing, GaAs resonator, optomechanical coupling, transient dynamics.**

I. Introduction

RECENTLY, the research and development of RC has greatly promoted its applications in dealing with various temporal tasks efficiently [1] [2] [3]. The most attractive RC model is the one introduced in Ref [4], in which only one nonlinear element was used to replace the large number of neurons in traditional reservoirs. So far, RC implementations using spintronic devices [5], photonic devices [6], memristors [7], microelectromechanical system (MEMS) resonators [8] have been investigated and realized. In those work, the RC realization using MEMS resonators is particularly of great practical significance. MEMS resonators have advantages of compact and low power consumption, which lead to many applications in Internet of Things (IoT), autonomous systems, mobile and wearable electronic devices [9]. To successfully implement the above mentioned RC model, it is crucial to make the nonlinear element-"computing substrates", exhibiting sufficient nonlinear dynamics and fading memory characteristics. However, the MEMS resonator currently adopted, e.g., Duffing resonator, lacks enough non-linearity required to better satisfy the RC operation, so that additional circuit designs such as time-delay feedback will be needed [10]. Moreover, the input signal to MEMS resonator is limited to be electrical, which hinders the application of RC from processing the information carried by light.

L. J and Z. L are with the College of Integrated Circuit Science and Engineering, Nanjing University of Posts and Telecommunications, Nanjing 210023, China; L. L is with College of Engineering, Swansea University, Swansea SA1 8EN, United Kingdom

Leisheng Jin is the corresponding author. E-mail: jinls@njupt.edu.cn

Manuscript received xx xx, xxxx; revised xx xx, xxxx.

In this work, we propose a novel NEMS GaAs resonator-based platform to implement RC. The resonator is doubly clamped bilayer beam so that it can be used for achieving cavity-free optomechanical coupling. Therefore the proposed RC is able to process information carried by light using the optomechanical coupling. This will increase RC efficiency and scope. Moreover, the light signals can make the resonator exhibit richer non-linearity leading to enhanced memory, improving the RC's performance. In the main text, a multi-physical dynamic model that incorporates optical, mechanical, and electrical modes is firstly developed for describing the nonlinear characteristics of the device, based on which the principle for realizing of RC is proposed. Then, the memory capacity of this RC through two benchmarks is verified. Subsequently, investigations on how the transient dynamical response affects the RC performance are conducted, followed by a comprehensive study on hyperparameters. The work sheds light for the development of a new generation of smart NEMS with built-in data processing capabilities.

II. Device Modeling and RC Working Principle

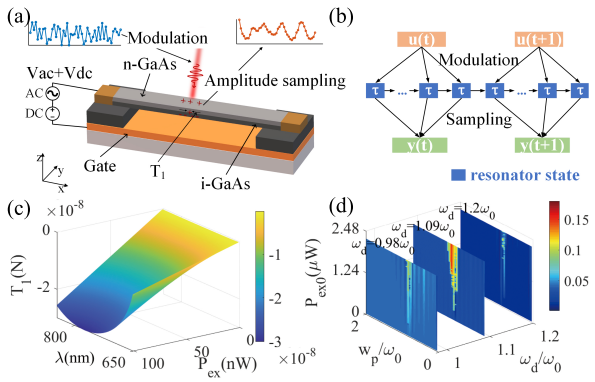

Fig. 1. (a) The proposed GaAs resonator for implementing RC; (b) Schematic description of RC working principle; (c) Laser-induced tension T_1 under different laser power and wavelength; (d) The calculation of laser-controlled amplitude of the GaAs resonator.

The proposed GaAs resonator for implementing RC is shown in Fig.1(a). Its dynamics can be modulated by laser injection via optopiezoelectric effect, which provides the foundation for processing the information carried by light. The device consists of a doubly-clamped GaAs beam with one third of its thickness as N-type (Si) doped and the rest as intrinsic. In the heterostructure, the Si doping and the pinning of the Fermi level can induce a built-in field in the direction perpendicular to the surface. Electron-hole pairs in the N layer generated by the optical absorption can be separated by this built-in field.

The charge separation leads to the optopiezoelectric effect, i.e., T_1, as indicated by the black arrow in Fig.1(a) because of the nonzero piezoelectric constant ($D \neq 0$) in GaAs material. The electromechanical driving force for the resonator is applied through an AC and DC gate voltage, i.e., $V_{dc} + V_{ac}$, where V_{ac} is with frequency ω_d. According to Euler-Bernoulli beam theory, the displacement W of the resonator is given by:

$$EI\frac{\partial^4 W}{\partial x^4} + \rho A\frac{\partial^2 W}{\partial t^2} + c_d\dot{W} - \left[T_0 + T_1 + \frac{EA}{2L}\int_0^L \left(\frac{\partial W}{\partial x}\right)^2 dx\right]\frac{\partial^2 W}{\partial x^2} = F_E \quad (1)$$

where E is Young's modulus, I is the area moment of inertia, ρ is the density, $A = W_d \times T_d$ is the cross-sectional area with W_d and T_d representing the width and thickness of the beam, respectively. L is the length of the beam. T_0 represents the initial tension in beam. F_E is distributed force applied on the beam, which can be expressed as:

$$F_E = -\pi\varepsilon V^2(t)/\left[(W+d)(ln(4(W+d)/r))^2\right] \quad (2)$$

where ε is dielectric constant of the gaseous medium surrounding the resonator, d is initial distance between the beam and the gate. The Eq.(2) can be further simplified by omitting the static and non-resonant terms based on approximation that the displacement is much smaller than the gap d. The damping ratio $c_d = -(\pi P d)/(4v_T)$, where P is the air pressure and $v_T = \sqrt{k_B T_k/m}$ represents the air molecule velocity at temperature T_k. To calculate the Eq.(1), the Galerkin's method [11] will be employed, based on which the displacement $W(x,t)$ can be substituted by: $W(x,t) = z(t)\phi(x)$, where $\phi(x)$ and $z(t)$ are the deflection eigenmode and displacement at the center point of the beam, respectively.

It is also of necessity to calculate the laser-induced tension T_1. According to the Fermi's golden rule [12], the transition rate happening per unit volume of material per second is:

$$R_{\uparrow(\downarrow)}(\omega) = \frac{4\pi}{\hbar}\left(\frac{qA_0}{2m}\right)^2 \left\langle |\hat{\overrightarrow{p}}_{cv}\cdot\hat{n}|^2\right\rangle \int_{FBZ}\frac{d^3\overrightarrow{k}_i}{(2\pi)^3}\cdot f_{v(c)}(\overrightarrow{k}_i)[(1-f_{c(v)}\overrightarrow{k}_i)\delta(E_c(\overrightarrow{k}_i) - E_v(\overrightarrow{k}_i) - \hbar\omega) \quad (3)$$

where $R_{\uparrow(\downarrow)}$ represents stimulated absorption and emission, respectively. The $f_v(\overrightarrow{k}_i)$ and $(1-f_c\overrightarrow{k}_i)$ represent the probability of an electron and hole in valence band and conduction band. The term $|\hat{\overrightarrow{p}}_{cv}\cdot\hat{n}|^2$, as the squared momentum matrix element, can be replaced by the average value of GaAs: 3.9×10^{-30}. The m and q are static mass and unit charge of an electron. E_v and E_c correspond to GaAs's top of the valence band and bottom of the conduction band, respectively.

The net photon absorption rate is then obtained as: $\alpha(\omega) = (R_\uparrow(\omega) - R_\downarrow(\omega))/(n_p c/n_g^M)$, where c/n_g^M is the velocity of the photons with c and n_g^M representing the velocity of light and the refractive index of GaAs, respectively. n_p is number of photons per unit volume, which is related with vector potential by $n_p = (1/2)(\omega^2/\hbar\omega)nn_g^M\varepsilon_0|\overrightarrow{A}_0|^2$.

The rate of carrier generation in the N-GaAs layer is further given by: $G_{eh} = P_{ex}\lambda_{ex}/c_1(1-e^{-\alpha(\omega)t_1})$, where P_{ex} and λ_{ex} are power and wavelength of injecting laser, respectively. c_1 is constant and t_1 is the thickness of N-GaAs layer. The number of generated electron-hole pairs are decided by the rate equation: $dn/dt = G_{eh} - n_{eh}/\tau$, where τ is the nonradiative recombination lifetime. Finally, the induced optopiezoelectric force can be calculated by: $T_1 = n_{eh}D$.

Based on the above modeling procedure, we firstly calculate the laser-induced tension T_1 when light power P_{ex} and wavelength λ_{ex} varying in [1 100]nW and [650 1250]nm, respectively. The laser driving power is applied in the form of $P_{ex} = P_{ex0}sin(\omega_p t) + P_{ex0}^{bias}$ with P_{ex0} and ω_p representing the amplitude and power modulation frequency. The P_{ex0}^{bias} is the predefined bias. Other parameters are taken as follows: $L = 3\times10^3$nm, $W_d = 150$nm, $T_d = 50$nm, $E = 85.5\times10^9$Pa, $T_0 = 3\times10^9$nN, $D = -1.35\times10^{-12}$C/N, $\tau = 1.6\times10^{-7}$s, $n_g^M = 3.9476$, $V_{dc} = V_{ac} = 5$V, and the result is shown in Fig.1(c). $X = x/d$ and $T = \omega_0 t$ are adopted during all the simulations for nondimensionalizing. The $\omega_0 \approx 1.467\times10^8$ Hz is resonant frequency of the resonator. d is set to be 200 nm. Investigations on how the key parameters including w_p, P_{ex0} and ω_d affect the nonlinear dynamics of the resonator are conducted. Three typical slices when the ω_d is set around the natural frequency ω_0 are given in Fig.1(d), in which it is seen the typical nonlinear "tongue" occurs at $w_p \approx 2\omega_0$.

An efficient RC using just one single GaAs resonator without time-delayed feedback can be realized. As shown in Fig.1(b), the proposed implementation of RC is composed of four phases: (1) input masking, (2) amplitude sampling, (3) readout regression and (4) prediction. In (1), the information $\boldsymbol{u}(k)$, where $k = 1, 2, 3...n$ denotes the discrete time step, is masked by a N-dimensional vector $\boldsymbol{Mask}$ to have $\boldsymbol{P_{ex0}}$, i.e.,: $\boldsymbol{P_{ex0}} = \boldsymbol{Mask}\times\boldsymbol{u} + \boldsymbol{P_{ex0}^{bias}}$, which will be superimposed on the amplitude of the injected laser power. In (2), the response of resonator is periodically sampled to have the output sequence $\boldsymbol{S}$. In (3), the $\boldsymbol{S}$ is trained targeting at the expected signal $\boldsymbol{y}$ through ridge regression, i.e., $\boldsymbol{W_{out}} = \boldsymbol{y}\boldsymbol{S}^T(\boldsymbol{S}\boldsymbol{S}^T + \lambda\boldsymbol{I})^{-1}$, where $\boldsymbol{I}$ is an identity matrix and λ is ridge parameter used for preventing over-fitting. The output value of the RC is given by: $\boldsymbol{y}(k) = \boldsymbol{W_{out}}\boldsymbol{S}(k)$. During The phases of (1)-(3), the information carried by light is input into resonator through masking, and the response of the resonator is sampled and trained to have the desired output. After training, the RC platform can run itself to predict signal based on the derived $\boldsymbol{W_{out}}$ in phase (4).

III. Simulation with Benchmark Tasks

To validate the prediction ability of the proposed RC, the NARMA benchmark task which can be used for measuring RC's memory capacity [4] is adopted, which is given by: $\boldsymbol{y}(k) = 0.3\boldsymbol{y}(k-1) + 0.05\boldsymbol{y}(k-1)(\sum_i^{n-1}\boldsymbol{y}(k-i-1)) + 1.5\boldsymbol{u}(k-n+1)\boldsymbol{u}(k) + 0.1$, where the input $u(k)$ is generated from an uniform density in $[0, 0.5]$, and the $\boldsymbol{y}$ is function of $\boldsymbol{u}(k)$. The n is a positive integer indicating how many steps delayed to the current state at k. The $\boldsymbol{u}(k)$ is then seen as the information carried by the laser, and a sample $\boldsymbol{u}(k)$ with a length of 100 is used to train the resonator according to the procedure described above. After training, a desired $\boldsymbol{W_{out}}$ is obtained, based on which we can test if the resonator-based RC can output signal equaling to the real $\boldsymbol{y}$ as $\boldsymbol{u}(k)$ is varying in a new range adjacent to the one in training

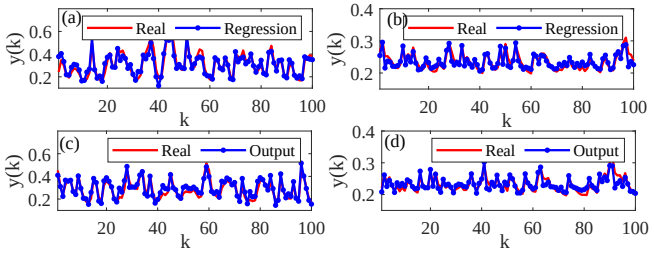

Fig. 2. (a) and (c): The training and testing results of the NARMA2 task; (b) and (d): The training and testing results of the second-order nonlinear dynamic task.

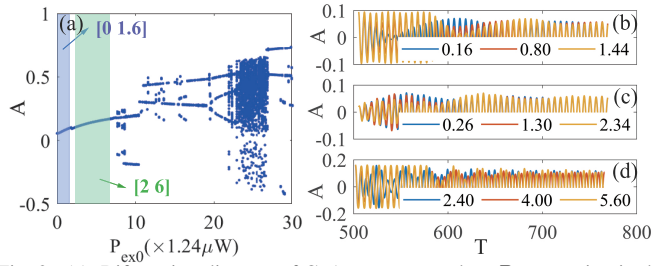

Fig. 3. (a): Bifurcation diagram of GaAs resonator when P_{ex0} varying in the range of $[0.1, 30] \times 1.24\mu W$ with $w_p = 2\omega_0$; (b)-(d): Results of resonator's transient dynamical responses under laser power setting in different P_{ex0} ranges consist with the shaded areas in (a).

phase. The simulation results are presented, respectively, in Fig.2(a) and (c). The NMSE is further adopted to quantitatively characterize the performance, which is expressed as: $NMSE = \sum_k (\boldsymbol{p}(k) - \boldsymbol{y}(k))^2 / \sum_k \boldsymbol{p}^2(k)$, where $\boldsymbol{p}(k)$ is the real signal and $\boldsymbol{y}(k)$ is the output signal. It can be calculated that the NMSE of the proposed RC realization can reach as low as 2.1×10^{-3}, that is one order of magnitude lower than the latest reported result (5.1×10^{-2}) [13]. Moreover, the second-order nonlinear dynamic task expressed by: $\boldsymbol{y}(k) = 0.4\boldsymbol{y}(k-1) + 0.4\boldsymbol{y}(k-1)\boldsymbol{y}(k-2) + 0.6\boldsymbol{u}^3(k-n+1) + 0.1$, is also used for validating the RC [14], and the testing results are given in Fig.2(b) and (d), in which the proposed RC again shows its outstanding memory capability with NMSE reaching 1.4×10^{-3}, lower than the result reported in [1]. A more comprehensive result of NMSE score of the NARMA benchmark subject to different sampling time and parameter settings of the injected laser is given in Fig.4 (a).

Essentially, the transient dynamical response of the resonator caused by laser plays a crucial role for implementing the RC. To have an insight, we firstly calculate the bifurcation diagram as shown in Fig.3(a). It can be seen that the resonator can exhibit rich dynamics including chaos under different laser driving powers. The shaded regions covering the coefficient range of [0, 1.6] and [2, 6] indicate the region at which the RC performs better and relatively poorer, respectively.

To further clarify how the laser affects the information processing capability, the transient dynamical responses of the resonator under different laser injections are investigated as shown in Fig.3(b)-(d). Take the Fig.3(b) for example, we assume that the resonator starts at the same initial state, and then its responses to three laser injections with different power ($P_{ex0} = 0.16 \times 1.24\mu W$, $0.80 \times 1.24\mu W$, $1.44 \times 1.24\mu W$) are calculated. One can see that the resonator immediately exhibits different transient dynamics. Then, we let the resonator in each of the three cases running for 12 vibration periods first, and apply another common laser with power equaling to $0.16 \times 1.24\mu W$. It can be seen that the different dynamics of the resonator induced by the first round of laser injections are gradually becoming synchronized. The similar transient dynamical response is also found with P_{ex0} increased to the range of $[0, 2.6] \times 1.24\mu W$ (Fig.3(c)). However, when the P_{ex0} in the first round of laser injections is increased to the range of $[2, 6] \times 1.24\mu W$ (Fig.3(d)), the synchronized dynamics after first round of laser injections cannot be reached, and on the contrary the phase of the transient dynamical response show discrepancies. E.g., the phase of the curve: 4.00, driven by $4.00 \times 1.24\mu W$ in the first round of injection, is 180 degree lag-behind with other two curves. The out-of-sync transient dynamical responses in this case leads to the reduction of the effective states used for conducting readout regression. This can explain why the NMSE of NARMA task is different when the resonator working with different laser drivings.

Finally, the effects of hyperparameters including nodes number, training length, sampling time and delay parameter in NARMA are investigated as shown in Fig.4. The Fig.4(a) shows the NMSE of NARMA-2 under different sampling time and systems parameter set (b: $P_{ex0} = (0-1.6) \times 1.24\mu W$ and $\omega_p = 2\omega_0$; c: $P_{ex0} = (0-2.6) \times 1.24\mu W$ and $\omega_p = 2.4\omega_0$; d: $P_{ex0} = (2-6) \times 1.24\mu W$ and $\omega_p = 2\omega_0$.). It is seen that the RC can perform the best by setting laser power in the parameter set of b and c and sampling time as $1/\omega_0 \times 2^n$ (n=[-3, 1]). Fig.4(b) and (c) show the NMSE of NARMA-2 and NARMA-10, respectively, with different sampling time and mask length. Fig.4(d) shows a more general result of which the NMSE of NARMA-N ($N = 1, 2..10$) task subject to different training lengths of an input sequence is investigated, where the NMSE can be further decreased with longer training obviously only for $N < 3$. Other factors such as signal-to-noise ratio and practical sampling means could affect the RC performance.

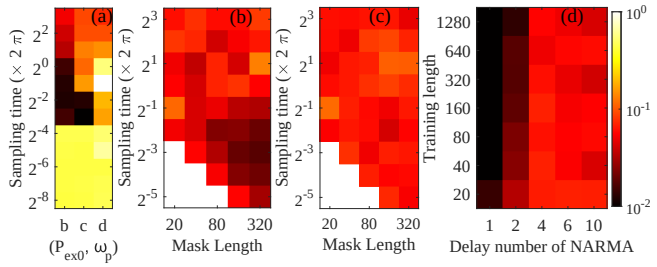

Fig. 4. The NMSE of NARMA2 with RC implemented using different hyperparameters. (a): NMSE vs (sampling time and parameter set of (P_{ex0}, ω_p)); (b) and (c): NMSE of NARMA-2 and NARMA-10 with different sampling time and mask length; (d): NMSE of NARMA-N ($N = 1, 2..10$) task subject to different training length.

IV. Conclusion

A novel RC platform based on NEMS GaAs resonator is proposed. The RC construction is distinctive in that it can efficiently process signal carried by light, avoiding the optical cavity and additional time-delay feedback designs. Benchmark tasks have been employed to verify its state-of-art performance. The interplay between the laser-mediated transient dynamics and the RC's performance is discussed. The work advances the field by introducing the concept of laser-driven mechanical RC.

REFERENCES

[1] C. Du, F. Cai, M. A. Zidan, W. Ma, S. H. Lee, and W. D. Lu, "Reservoir computing using dynamic memristors for temporal information processing," *Nature Communications*, vol. 8, p. 2204, 2017, doi:10.1038/s41467-017-02337-y.

[2] V. Pyragas and K. Pyragas, "Using reservoir computer to predict and prevent extreme events," *Physics Letters A*, vol. 384, no. 24, p. 126591, 2020, doi:10.1016/j.physleta.2020.126591.

[3] J. Pathak, B. Hunt, M. Girvan, Z. Lu, and E. Ott, "Model-free prediction of large spatiotemporally chaotic systems from data: A reservoir computing approach," *Phys. Rev. Lett.*, vol. 120, p. 024102, Jan 2018, doi:10.1103/PhysRevLett.120.024102.

[4] L. Appeltant, M. Soriano, G. Van der Sande, J. Danckaert, S. Massar, J. Dambre, B. Schrauwen, C. Mirasso, and I. Fischer, "Information processing using a single dynamical node as complex system," *Nature Communications*, vol. 2, p. 468, 2011, doi:10.1038/ncomms1476.

[5] J. Grollier, D. Querlioz, and K. e. a. Camsari, "Neuromorphic spintronics," *Nature Electronics*, vol. 3, p. 360–370, 2020, doi:10.1038/s41928-019-0360-9.

[6] W. Du, C. Li, Y. Huang, J. Zou, L. Luo, C. Teng, H.-C. Kuo, J. Wu, and Z. Wang, "An optoelectronic reservoir computing for temporal information processing," *IEEE Electron Device Letters*, vol. 43, no. 3, pp. 406–409, 2022, doi:10.1109/LED.2022.3142257.

[7] S. Wen, R. Hu, Y. Yang, T. Huang, Z. Zeng, and Y.-D. Song, "Memristor-based echo state network with online least mean square," *IEEE Transactions on Systems, Man, and Cybernetics: Systems*, vol. 49, no. 9, pp. 1787–1796, 2019, doi:10.1109/TSMC.2018.2825021.

[8] B. Barazani, G. Dion, J.-F. Morissette, L. Beaudoin, and J. Sylvestre, "Microfabricated neuroaccelerometer: Integrating sensing and reservoir computing in mems," *Journal of Microelectromechanical Systems*, vol. 29, pp. 338–347, 2020, doi: 10.1109/JMEMS.2020.2978467.

[9] G. Pillai and S.-S. Li, "Piezoelectric mems resonators: A review," *IEEE Sensors Journal*, vol. 21, no. 11, pp. 12 589–12 605, 2021, doi:10.1109/JSEN.2020.3039052.

[10] L. Jaurigue and K. Lüdge, "Connecting reservoir computing with statistical forecasting and deep neural networks," *Nature Communications*, vol. 13, no. 227, 2022, doi:10.1038/s41467-021-27715-5.

[11] M. Şimşek, "Nonlinear free vibration of a functionally graded nanobeam using nonlocal strain gradient theory and a novel hamiltonian approach," *International Journal of Engineering Science*, vol. 105, pp. 12–27, 2016, doi: 10.1016/j.ijengsci.2016.04.013.

[12] E. Ciancio, R. Iotti, and F. Rossi, "Gauge-invariant formulation of fermi's golden rule: Application to high-field transport in semiconductors," *EPL (Europhysics Letters)*, vol. 65, no. 2, p. 242, 2004, doi:10.1209/epl/i2003-10065-7.

[13] J. Sun, W. Yang, T. Zheng, X. Xiong, Y. Liu, Z. Wang, Z. Li, and X. Zou, "Novel nondelay-based reservoir computing with a single micromechanical nonlinear resonator for high-efficiency information processing," *Microsystems & Nanoengineering*, vol. 7, p. 83, 2021, doi:10.1038/s41378-021-00313-7.

[14] A. Atiya and A. Parlos, "New results on recurrent network training: unifying the algorithms and accelerating convergence," *IEEE Transactions on Neural Networks*, vol. 11, no. 3, pp. 697–709, 2000, doi:10.1109/72.846741.